

Breakdown of the Kondo insulating state in SmB_6 by introducing Sm vacancies.

Michael E. Valentine, Seyed Koohpayeh, W. Adam Phelan, Tyrel M. McQueen, and Natalia Drichko*
*Institute for Quantum Matter and Department of Physics and Astronomy,
 Johns Hopkins University, Baltimore, MD 21218, USA*

Priscila F. S. Rosa and Zachary Fisk
*Department of Physics and Astronomy, University of California, Irvine, California 92697, USA
 (Dated: October 31, 2021)*

SmB_6 is a proposed topological Kondo insulator where the presence of topological nontriviality can be tuned by variations in the Sm valence. Experimentally, Sm valence can be changed by tuning stoichiometry of SmB_6 . We show that Raman scattering can detect vacancies down to 1% of Sm sites in SmB_6 crystal by probing the intensity of defect-induced scattering of the acoustic phonon branch at 10 meV. In the electronic Raman spectra of SmB_6 at temperatures below 130 K, we observe features developing in A_{1g} and E_g symmetries at 100 and 41 meV which we assign to excitations between hybridized bands, and depressed spectral weight below 20 meV associated with the hybridization gap. With the increased number of Sm vacancies up to 1% we observe an increase of spectral weight below 20 meV showing that the gap is filling in with electronic states. For the sample with the lowest number of vacancies the in-gap exciton excitations with long lifetimes protected by hybridization gap are observed at 16-18 meV in E_g and T_{2g} symmetries. These excitations broaden as a decrease in the lifetime with increasing number of vacancies and are quenched by the presence of in-gap states at concentration of Sm vacancies of about 1%. Based on this study we suggest that only the most stoichiometric SmB_6 samples have a bulk gap necessary for topological Kondo insulators.

I. INTRODUCTION

Much recent research is aimed on experimental realization of a new state of matter, topological insulator (TI), where topologically protected metallic surface states appear due to a surface crossing of inverted bands in the bulk. While the TI state was initially proposed for band insulators, it was realized that Kondo insulators also can be a source of topologically invariant surface state [1–3]. SmB_6 is one of the materials which are suggested to show properties of topological Kondo insulator (TKI). This material has been studied extensively due to its mixed valence and Kondo insulating properties. A presence of the metallic surface states reveal itself as a plateau in the d.c. resistivity temperature dependence below 5 K which has been attributed to surface conduction [4–6]. Interpretation of this metallic surface states varies from TI state [4, 6] to polarity-driven surface states [5, 7].

The basic requirement for TI state to exist is a presence of inversion of the energy bands forming the respective insulating gap. In SmB_6 , a gap opens at the Fermi level due to hybridization between $4f$ and $5d$ electronic bands below 70 K (below 150 K according to Ref. 8). The size of the hybridization gap has been estimated by several techniques. Optical measurements suggests a gap of 16-19 meV with an impurity band at 3-5 meV [9–12], photoemission at 18 meV [8], point-contact spectroscopy at 21 meV with an in-gap band at 4.5 meV below the conduction band [13, 14], and DC resistivity estimates the activation energy at 3.5 meV [4]. Several band structure

calculations predict a gap opening due to hybridization of $4f$ and $5d$ orbitals, with band inversion necessary for topological nontriviality at the X-point in the Brillouin zone (BZ) [15, 16]. A recent neutron scattering study [17] gives evidence of band inversion at around X and R points of the Brillouin zone.

It is proposed that a change in the average Sm valence can cause a transition from a strong topological insulator state to a trivial band insulator.[3] An introduction of Sm vacancies through increasing Sm deficiency is a means for shifting average Sm valence. This can be achieved in a controlled way along the length of a floating zone (FZ) grown crystal [18]. At the transition between the TI and trivial states the gap should close, but for the situations, where the symmetry of the system is broken [19]. The aim of our work was to follow a change of the bulk gap with a change of average Sm valence tuned by the number of Sm vacancies. To do this we use Raman spectroscopy, which can probe bulk electronic structure through measuring intra- and inter-band excitations [20, 21]. Low frequency Raman scattering measurements already proved to be useful in studies of the hybridization gap and in-gap states for Al-flux grown SmB_6 samples [22, 23]. Here we present a wide energy range Raman study of SmB_6 samples with a variation in number of Sm vacancies, which allows us to get rich information on the phonon and electronic spectrum of these samples.

We demonstrate that phonon Raman scattering is a sensitive tool to characterize the presence and relative amount of Sm vacancies in SmB_6 crystals. In the electronic Raman response at low temperatures for all the samples we observe features associated with the excitations over hybridization gap. We show that the presence of even 1% of Sm vacancies affects the hybridization gap

* Corresponding author: drichko@jhu.edu

by filling it with in-gap states. In samples with a negligible number of Sm vacancies, we observe features originating from the in-gap excitonic level.[17, 24, 25] The exciton feature is quenched in the samples with about 1% Sm vacancies due to the presence of the in-gap impurity states.

II. EXPERIMENT

A. Crystal growth

In this study we used single crystals of SmB_6 grown by Al flux and floating zone (FZ) techniques. Al flux- SmB_6 samples were grown by standard Al flux technique. For our study, we selected a crystal, Al Flux- SmB_6 , found from Raman measurements to have the fewest Sm vacancies and comparable linewidths of boron Raman active phonons to FZ samples. A value of the line width of boron phonons as a parameter to characterize the quality of SmB_6 samples and the degree of structural variation within Al flux grown samples will be discussed elsewhere [26].

FZ single crystals of SmB_6 were grown using the optical floating zone technique [5, 18] and are representative of "typical" SmB_6 crystals described in these papers. A previous study shows increasing presence of Sm vacancies along the length of a single FZ crystal due to vaporization of the rod materials into a Sm rich mixture and can be characterized by a systematic decrease in lattice parameters. For our study we used two samples, cut from the most stoichiometric (FZ SmB_6 -Pure) and most Sm deficient (FZ SmB_6 -Defc) end of the rod. Based on powder diffraction measurements of the lattice parameters in comparison to previous results for non-stoichiometric SmB_6 , we estimate the most deficient sample (FZ SmB_6 -Defc) to be about 1% deficient [18]. Magnetization measurements for the two FZ-grown samples did not show a significant difference in average magnetic moment which could arise from larger differences in the number of Sm vacancies [27].

B. Raman measurements

Raman measurements were performed using a Horiba Jobin-Yvon T64000 triple monochromator spectrometer in the pseudo-Brewster angle geometry for energies from 2.5 meV (20 cm^{-1}) to 500 meV (4000 cm^{-1}) with resolution up to 0.25 meV (2 cm^{-1}). A Coherent Ar^+ laser was used as a source for excitation light with wavelengths 488 nm and 514 nm which was focused on the samples with a spot size of 50 by 100 μm . Penetration depth of the light at 514 nm is estimated to be of the order of 100 nm. The measurements were performed on cleaved surfaces which were exposed to atmosphere before the measurements. No Raman evidence of samarium oxide which

Polarization	e_i, e_s geometry	Symmetry (O_h)
(x, x)	$c(aa)\bar{c}$	$A_{1g}+E_g$
(x, y)	$c(ab)\bar{c}$	T_{2g}
(x', x')	$c(\frac{a+b}{\sqrt{2}}, \frac{a+b}{\sqrt{2}})\bar{c}$	$A_{1g}+1/4E_g+T_{2g}$
(x', y')	$c(\frac{a+b}{\sqrt{2}}, \frac{a-b}{\sqrt{2}})\bar{c}$	$3/4E_g$

TABLE I. Polarizations of the measured Raman scattering spectra of SmB_6 , the geometry of the measurements, and the probed irreducible representations for each polarization.

typically appears on the surface of the samples exposed to air was detected in the measured Raman spectra.

Measurements were performed over a temperature range of 10 to 300 K using a Janis ST-500 cold finger cryostat with samples affixed to the cold finger using silver paint. Laser heating was estimated to be 10 K at 10 mW, and the power was reduced to reach the lowest temperatures. All spectra were corrected by the Bose-Einstein thermal factor. To compare the results for different samples the spectra were normalized on the intensity of the 1143 cm^{-1} phonon to compensate for the small differences in intensity due to the variation in the quality of the cleaved surfaces.

SmB_6 has $Pm\bar{3}m$ cubic symmetry of the unit cell, O_h point group symmetry. The crystals were oriented using X-ray diffraction and polarization-dependent Raman scattering measurements. The temperature dependent measurements were performed in (ab) plane with the orientations of the electrical field of the incident light e_i and electrical vector of the scattered light e_s listed in Table I. The large acceptance angle of the analyzing optics results in some additional signal from other polarizations. In the table we also present the irreducible representations of the O_h point group probed in these polarizations. Of these, E_g corresponds to B_{1g} , and T_{2g} corresponds to B_{2g} irreducible representations of D_{4h} group, for which calculations of electronic Raman scattering were performed[20, 28].

III. RESULTS

The Raman spectra of SmB_6 consist of relatively narrow phonons peaks superimposed on the electronic background. Most of the features of the phonon spectrum have been previously studied [22, 23, 29–32]. In Sec. III A, we discuss how previously unidentified defect-induced phonon scattering can be used to extract the information on Sm vacancies in the studied samples of SmB_6 . The electronic Raman response for the samples with different numbers of Sm vacancies is discussed in Sec. III B.

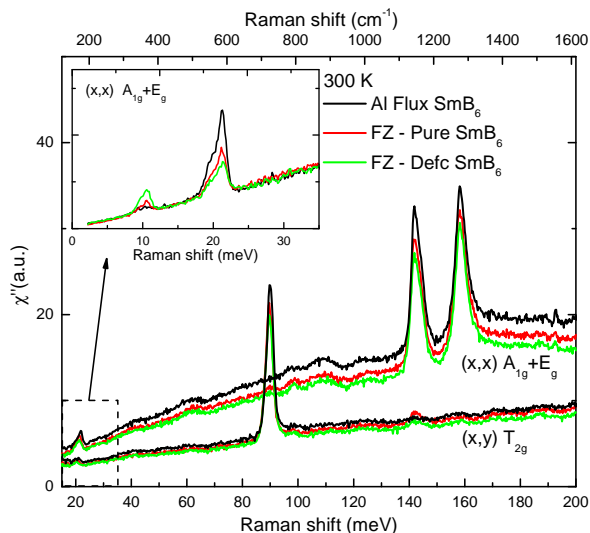


FIG. 1. Room temperature Raman spectra of the three studied SmB_6 samples with increasing number of Sm vacancies (Al Flux- SmB_6 , FZ SmB_6 -Pure, FZ SmB_6 -Defc) in (x, x) and (x, y) polarizations. The 3 first-order Raman active phonons appear at 89.6 meV (T_{2g}), 141.7 meV (E_g), and 158.3 meV (A_{1g}) are superimposed on a broad continuum of electronic scattering. Inset shows low-frequency (x, x) spectra of the samples. Two symmetry forbidden peaks appear at 10 meV and 21 meV correspond to defect-induced and two-phonon scattering, respectively.

A. Phonons

In the cubic unit cell of SmB_6 , the Sm ions are located at a center of inversion symmetry, and thus phonons involving this site are forbidden in the first order Raman spectrum. The three symmetry allowed Raman phonons seen as the intense relatively narrow features (see Fig. 1) are the T_{2g} symmetry phonon at 89.6 meV (723 cm^{-1}), E_g at 141.7 meV (1143 cm^{-1}), and A_{1g} at 158.3 meV (1277 cm^{-1}) exclusively involve motion of the atoms within the B_6 octahedra [31]. They are observed in polarizations corresponding to their symmetries and are well-known from other vibrational Raman studies of SmB_6 crystals [22, 23, 29, 31, 32]. The widths of the phonons are 2-4 meV which emphasizes the role of valence fluctuations and disorder in the crystals [33]. While Al-flux grown samples show variations among the first order B_6 octahedra phonon energies of 1 meV and linewidths 0.8 meV [26] for our measurements we chose the sample (Al Flux- SmB_6) with the lowest line width of boron phonons, which was an evidence of a minimized disorder in the sample. For this sample, the positions of the boron phonons coincide with that of the FZ-grown samples.

The phonon features at 10 and 21 meV (see Fig. 1) observed strongest in (x, x) polarization are assigned to phonons associated with Sm motion, which are Raman silent for the $Pm\bar{3}m$ symmetry of the unit cell. Pre-

viously both features were associated with two-phonon scattering.

The 21 meV feature has two components, the sharper peak at 21.9 meV that has maximum intensity in (x, x) polarization, and a wider polarization-independent component with a maximum at 20.3 meV. The intensity of this feature as a whole decreases on going from Al flux SmB_6 to FZ-Defc- SmB_6 sample (see inset in Fig. 1), but for all of the samples the feature decreases in intensity on cooling. The feature was previously attributed to the two-phonon scattering from acoustic phonons [23, 30], based on its temperature dependence. Optical phonon branches, as well as a non-dispersive mode of a phonon coupled to the valence fluctuations are observed by neutron scattering in the same energy range [34, 35], however, more experimental data is necessary to understand if those affect the Raman intensity.

The assignment of the feature at 10 meV to two-phonon scattering [31, 32] does not account for the temperature dependence which follows a first-order thermal factor $\frac{1}{1 - e^{-\frac{\hbar\omega}{kT}}}$, and the lack of singularities in phonon density of states at half this energy necessary for strong two-phonon scattering [34]. We instead attribute this feature to acoustic phonons, which become Raman active due to local symmetry breaking induced by the presence of Sm defects. This loss of translational invariance allows light scattering from all points within the BZ [33]. The relevant acoustic phonons with energies around 10 meV and a flat dispersion over the latter half of the BZ are observed in neutron scattering experiments [34]. The flat dispersion of this phonon is responsible for the relatively small line width of the Raman feature.

The Sm defect-induced phonon at 10 meV shows an increase in spectral weight with increasing Sm deficiency between the two FZ-grown samples (Fig. 1). While the increase of the number of Sm vacancies between these two samples is estimated to be less than 1%, the difference in the intensity of the Sm defect-induced phonon at 10 meV is about 1.5 times and can be easily detected. This shows that Raman scattering can be effectively used to characterize the number of Sm vacancies in SmB_6 samples. The intensity of 10 meV phonon has nearly zero spectral weight for the best Al Flux- SmB_6 sample, demonstrating that the sample has the lowest number of Sm vacancies. The intensity of this Sm symmetry-forbidden phonon allows us to order the three studied samples by increasing number of Sm vacancies from Al Flux- SmB_6 to FZ SmB_6 -Pure, and further to FZ SmB_6 -Defc. As the next step we follow the temperature dependence of electronic Raman scattering within this range of samples.

B. Electronic Raman scattering

In the Raman spectra of all three samples at 300 K, we observe electronic backgrounds which linearly increase in intensity with energy up to about 150 meV (1200 cm^{-1}) and stays constant at higher energies (see Fig. 1). The

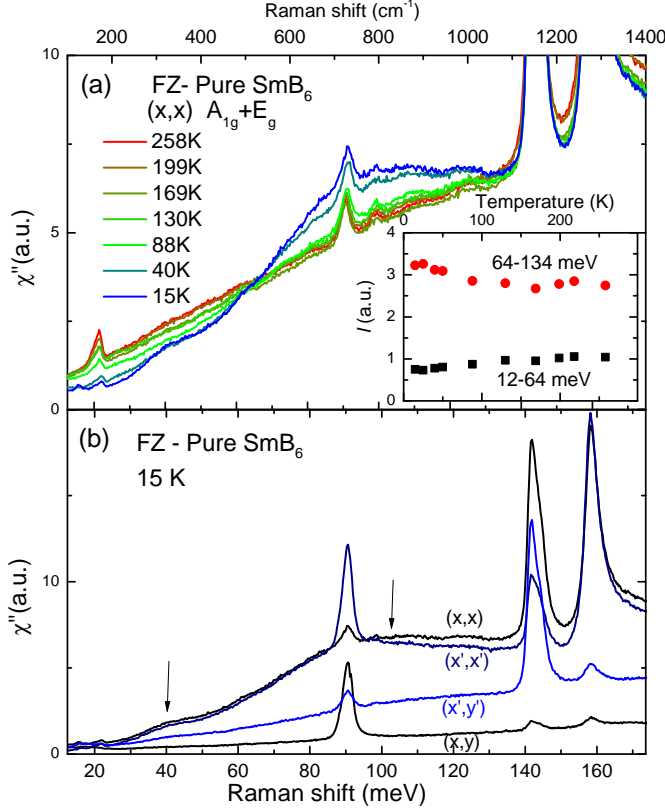


FIG. 2. (a) Temperature dependence of Raman spectra of the FZ SmB₆-Pure sample cooled from 300 K to 15 K in (x, x) polarization. Note redistribution of the spectral weight which occurs below 130 K to the frequencies above 100 meV, and below 50 K to the frequency range above 34 meV. The inset shows a temperature dependence of spectral weight $I(T) = \int_{\omega_0}^{\omega_1} \chi''(T, \omega) d\omega$ below ($\omega_0 = 12$ meV, $\omega_1 = 64$ meV) and above ($\omega_0 = 64$ meV and $\omega_1 = 134$ meV) the isosbestic point. (b) Raman spectra of FZ SmB₆-Pure sample at 15 K in (x', y') , (x', x') , (x, y) and (x, x) polarizations, see Table I. The temperature dependent response is most intense in (x', x') and (x, x) polarizations, suggesting that it belongs to A_{1g} symmetry.

background is observed in all four measured polarizations, though it is considerably weaker in (x, y) . This background is present in the spectra excited with 488 nm line as well, which suggest that it originates from electronic Raman scattering [21].

The changes observed in the Raman spectra of all the samples on cooling from 300 to 15 K are illustrated by the temperature dependence the response of the FZ SmB₆-Pure sample in (x, x) polarization presented in Fig. 2 (a). On decreasing temperatures below 130 K, we detect a spectral weight shift to frequencies above an isosbestic point of 64 meV. The resulting feature with a maximum at about 100 meV continues to develop down to 20 K.

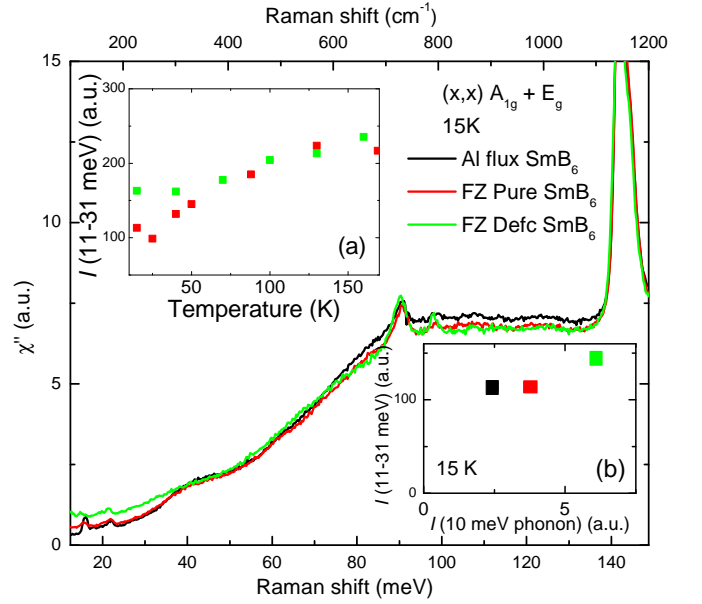


FIG. 3. Low-temperature Raman spectra of Al Flux-SmB₆, FZ SmB₆-Pure, and FZ SmB₆-Defc samples at 15 K in (x, x) polarization. Note an increase of in-gap intensity and smearing of 41 meV feature with the increase in Sm vacancies. (a) Temperature dependence of the spectral weight $I(T) = \int_{\omega_0}^{\omega_1} \chi''(T, \omega) d\omega$ below 31.5 meV in FZ SmB₆-Pure sample (red dots) vs FZ SmB₆-Defc sample (green dots). The difference becomes apparent below 50 K, where the 41 meV feature starts to develop in the spectra. (c) Spectral weight below 31.5 meV plotted against the intensity of the defect phonon. Note the increase of the low frequency spectral weight with the increase of the number of Sm vacancies.

We can follow the temperature dependence of the high-frequency feature by following the temperature dependence of the spectral weight $I(T) = \int_{\omega_0}^{\omega_1} \chi''(T, \omega) d\omega$ below ($\omega_0 = 12$ meV, $\omega_1 = 64$ meV) and above ($\omega_0 = 64$ meV and $\omega_1 = 134$ meV) the isosbestic point, $\chi''(T, \omega)$ is Raman intensity in arbitrary units. Another redistribution of the spectral weight occurs at temperatures below 50 K, resulting in a band at 41 meV with further suppression of the spectral weight below 34 meV. This lower-frequency effects are in general agreement with Ref. [22, 23], while the feature at about 100 meV was not yet discussed. The total spectral weight of the spectra below 134 meV (the sum of the two parts) is conserved, as expected for a system where a metal-insulator transition is driven by electronic correlations [36].

As seen from polarization dependence of the spectra at 15 K (Fig. 2 (b)), both features have the highest intensity in (x, x) and (x', x') , with somewhat lower intensity at the same frequencies observed in (x', y') . This shows that both features appear in A_{1g} and E_g symmetries at the same energies. In (x, y) polarization (T_{2g} symmetry, see Sec. II B) the Raman response in this frequency range is low and basically temperature independent, and neither of these two features are observed at 15 K.

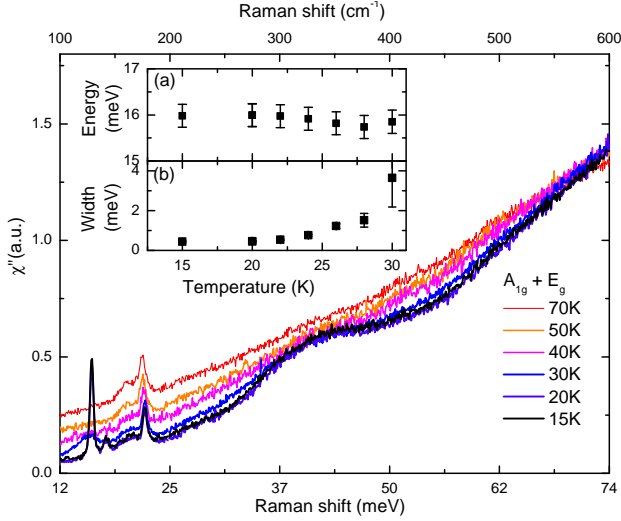


FIG. 4. Temperature dependence of the low frequency Raman response of Al Flux-SmB₆ sample in (x, x) polarization. The exciton feature appears below 30 K at 16 meV. The inset shows a change of the position and width of the exciton on cooling.

A similar changes of the spectra on cooling are observed in the other samples. We compare the (x, x) spectra at 15 K for the samples with different concentrations of Sm vacancies in Fig. 3. The position and intensity of the feature at 100 meV is the same for all measured samples. The feature at 41 meV gets smeared with an increase of the number of vacancies leaving some spectral weight at low frequencies. We follow this as the decrease of the spectral weight on cooling $I(T) = \int_{\omega_1}^{\omega_0} \chi''(T, \omega) d\omega$ between $\omega_0 = 11$ meV, $\omega_1 = 31.5$ meV for FZ SmB₆-Pure (red squares) and FZ SmB₆-Defc (green squares) in the inset (a) in Fig. 3. The spectral weight shows identical dependence on temperature in both samples down to approximately 50 K. Below this temperature no major changes occur in the low frequencies range for the FZ SmB₆-Defc sample, while the further decrease of the low frequency spectral weight is observed in FZ SmB₆-Pure sample. The resulting correlation between the number of vacancies estimated as the intensity of the 10 meV phonon $I(10 \text{ meV phonon})$ and the low frequency spectral weight $I(11-31 \text{ meV})$ is shown in the inset (b) of Fig. 3. With the decrease of the number of vacancies the low frequency spectral weight decreases.

While the low frequency spectral weight has similar values in FZ SmB₆-Pure and Al Flux-SmB₆ in the spectra of the Al Flux-SmB₆ sample at temperatures below 30 K the intensity is concentrated in the narrow features of in-gap excitations (see Fig. 4 and Fig. 5) observed both in (x, x) and (x, y) polarizations. Table II lists all of the in-gap features, including those in (x, y) polarization, and their symmetry assignment following Ref. [23]. The temperature behaviour followed in (x, x) polarization shows that the sharp peak forms when the spectral weight at

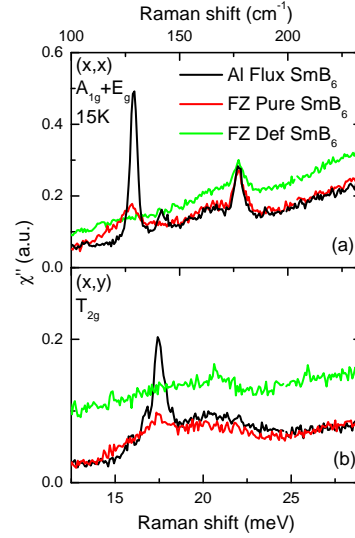


FIG. 5. Raman spectra in the frequency range of the exciton feature at 15 K for the measured samples, Al Flux-SmB₆, FZ SmB₆-Pure, and FZ SmB₆-Defc in (x, x) polarization (a) and (x, y) polarization (b).

Polariz.	Symm.	Al Flux		FZ Pure	
		Freq	Width	Freq	Width
(x, y)	T_{2g}	15.9 meV	0.7 meV		
(x, x)	E_g	16.0 meV	0.5 meV	15.6 meV	1.7 meV
(x, y)	T_{2g}	16.7 meV	0.7 meV		
(x, y)	T_{2g}	17.5 meV	0.7 meV	17.4 meV	1.5 meV

TABLE II. Polarization dependence, symmetry, frequency and width of the excitonic features observed in the samples with the smaller numbers of Sm vacancies (Al Flux-SmB₆ and FZ SmB₆-Pure) at 15 K.

low frequencies becomes sufficiently low, the frequency of the feature stays the same 16.0 meV, while the width decreases with temperature till it reaches the value of about 0.5 meV (see Fig. 4 (b)).

In the FZ SmB₆-Pure sample lower intensity and wider (1.7 meV) in-gap feature at 15.6 meV is superimposed on even wider (4.7 meV) background. The in-gap excitations are not observed in the spectra of the FZ SmB₆-Defc, where higher electronic scattering intensity is present at frequencies within the hybridization gap (Fig. 5).

IV. DISCUSSION

The excitations revealed in the low temperature Raman spectra are of electronic origin, and appear due to hybridization of $5d$ and $4f$ orbitals, as suggested by their temperature dependence and energy scale. The interpretation of the electronic Raman spectra can be made from

two points of view. The low temperature electronic Raman spectra can be compared to the band structure calculations, which take into account electronic correlations and hybridization of $5d$ and $4f$ bands, and reproduce the hybridization gap and band inversion in SmB_6 [3, 15, 16]. On the other hand, the change of the low-frequency electronic Raman spectra of SmB_6 on cooling, the formation of hybridization gap, and polarization dependence of the spectra can be compared to the calculations of electronic Raman spectra for a system with localization effects originating from electronic correlations[36].

The shift of the spectral weight to the higher frequencies on cooling indicates the formation of the insulating gap due to correlation effects, as was already discussed in connection with SmB_6 low frequency Raman spectra [36]. In our measurements, for all the samples the spectral weight is conserved above 105 meV (850 cm^{-1}), this cutoff indicating the energy range associated with the formation of the hybridization gap.

Of the band structure calculations, in particular that performed by LDA+Gutzwiller method presented in Ref. 16 provides bands energies which correspond well to the electronic excitations observed in our data at low temperatures. The calculations show the hybridized $5d$ and $4f$ bands, where $4f$ $j = 5/2$ band splits into two Γ_7^f and one Γ_6^f bands resulting in band inversion in the vicinity of the X point of the B.Z. and a formation of a semiconductor-like gap. The possible interband excitations would have energies close the 41 and 100 meV observed in our experiment (Fig. 3 in Ref. 16). Interestingly, optical conductivity also shows a broad peak at around 100 meV [11]. In inversion symmetric crystals Raman measurements should only probe electronic transitions from bands of the same parity while infrared is limited to bands of different parity. Here the mixed parity of the hybridized $5d$ - $4f$ orbitals in SmB_6 apparently allows this transition to appear in both measurements.

Depending on the measured polarization, Raman scattering probes electronic excitations at different parts of the B.Z. [20]. The response in A_{1g} probes the excitations over the whole B.Z. The 100 meV and 41 meV features appear with the highest intensity in A_{1g} symmetry. According to the calculations[16], the dispersions of the relevant bands along the Γ - X direction are relatively flat, and thus would result in peaks in the Raman response. E_g symmetry which corresponds to B_{1g} for D_{4h} point group probes the transitions around the X point and is expected to show Raman response due to correlation effects [28]. We do observe both features in E_g response at similar frequencies as in A_{1g} within the precision of the measurements, which is in agreement with the flat band dispersion.

Following the interpretation of the low temperature spectra within the band structure calculations [16], we would expect to observe a predicted much larger gap in T_{2g} symmetry, which probes the M point of the BZ. However, in this symmetry the Raman electronic background has low intensity which does not change with tempera-

ture (see Fig. 2 (b)). On the other hand, the Raman response due to correlation effects in T_{2g} which can be projected on B_{2g} for D_{4h} symmetry is predicted to be zero[28] in approximations of cosine bands. This absence of temperature-dependent response in T_{2g} can be taken as an evidence of the defining importance of the electronic correlations for the effects observed in SmB_6 spectra and a limitation of the band-structure approach.

The two features in the Raman spectrum at 100 and 41 meV associated with hybridization of the $5d$ and $4f$ orbitals start to develop at the relevant temperatures, 130 and 50 K. At low temperatures, the 100 meV feature has equal intensity in all three samples, as seen from Fig. 3. The differences in the low-frequency spectral weight between FZ SmB_6 -Pure and FZ SmB_6 -Defc samples appear only below 50 K (Fig. 3, inset (a)). The depressed Raman intensity below roughly 30 meV in A_{1g} and E_g symmetries in Al Flux- SmB_6 and FZ SmB_6 -Pure samples is a result of the opening of the hybridization gap. By evaluating in-gap spectral weight in the gap (Fig. 3(b)) we cannot distinguish the two samples with the least number of vacancies, Al Flux- SmB_6 and FZ SmB_6 -Pure while we observe a somewhat higher intensity in the spectra of FZ SmB_6 -Pure sample at low frequencies. With the increase of the number of Sm vacancies for the FZ SmB_6 -Defc sample an increase of the in-gap spectral weight and the respective decrease of the 41 meV band are detected. This increase of the amount of the in-gap spectral weight suggests that the hybridization gap is not opened completely in FZ SmB_6 -Defc sample.

At 15 K we observe the sharp in-gap excitations at about 16 meV in Al Flux- SmB_6 while in FZ SmB_6 -Pure spectra the same spectral weight is spread over wide frequency range in the gap, with a wide peak in the same range (Fig. 5). The excitation at 16 meV can be interpreted in terms of in-gap exciton. The respective excitonic level is proposed to be formed by electrons of hybridized bands in the gap as a result of strong electron-electron correlations and is protected from decay by the hybridization gap [25]. The excitonic feature was observed in neutron scattering measurements at finite momentum transfers with scattering intensity at the X and R high symmetry points of the BZ[17]. The most intense feature observed in Raman spectra belongs to E_g symmetry, which probes the excitation at the X point of the BZ[17]. Raman probes zero momentum transfer direct transitions, and thus the energies of these excitation of 16 meV is higher than that observed in neutron scattering at 14 meV at X point.

The multiple features of T_{2g} symmetry (Fig. 5, Table II) cannot be assigned to pure electronic response. The previous work[22, 23] proposes an alternative model for the multiple excitonic features which appear as a result of a splitting of crystal field levels by coupling with phonons[37]. According to the model, the feature at 16 meV in E_g symmetry has dominant electronic contribution, while multiple exciton-related features in T_{2g} symmetry have dominant phonon contribution [23].

The low line width of the excitonic features observed in the Al Flux-SmB₆ sample (0.5 meV) is evidence of an exceptionally long life time protected by the hybridization gap. The widening of the feature on the increase of the number of vacancies in FZ SmB₆-Pure shows that some electronic state are present within the gap energies and lead to the exciton decay. Respectively, no exciton features are detected in the spectra of FZ SmB₆-Defc since the gap is not fully opened in this material.

Our Raman results for FZ-grown samples are mirrored by transport measurements which show a decrease of the metallic-like plateau in resistivity at low temperatures and more insulating behavior for the FZ SmB₆-Pure samples compared to FZ SmB₆-Defc[18]. Such results emphasize the dramatic effect the presence of Sm vacancies has on the bulk hybridization gap necessary for the existence of KTI. While in the most stoichiometric samples (Al Flux-SmB₆ in this study) we find the hybridization gap fully opened and detect the presence of the in-gap exciton, which can be an evidence of the KTI state, even 1 % increase in the number of Sm vacancies due to the growth condition suppresses the development of hybridization gap and can eliminate the KTI state. The presence of Sm vacancies can introduce doping, but the effects of disorder also can be important. To probe the exact mechanism of an effect of Sm vacancies on the metallic low-temperature response of SmB₆ one needs to use frequency-dependent optical techniques which in contrast to Raman scattering have an ability to directly probe the bulk charge carriers.

V. CONCLUSIONS

We present Raman scattering study of SmB₆ samples with different numbers of Sm vacancies. We show that Raman scattering is an extremely sensitive method to characterise the number of Sm vacancies by the estimation of the intensity of the Raman-forbidden phonon of Sm at 10 meV, which appears in the spectra due to the local symmetry breaking by Sm vacancies.

In the Raman spectra below 130 K for all the samples we observe a development of the electronic features at 100 and 41 meV in A_{1g} and E_g symmetries. Based on the recent band structure calculations we assign the features to the excitations between the bands in the electronic structure which appear due to hybridization between 5*d* and 4*f* orbitals. In turn, our Raman study provides experimental data on electronic structure of SmB₆ to support the calculations. In this interpretation, the band at about 41 meV is the excitation across the hybridization gap. While the feature at 100 meV develops equally in all the samples, with an increasing of the number of Sm vacancies up to approximately 1% the hybridization gap stays filled with states without a detectable shift in the size of the gap.

For the samples with the low number of Sm vacancies in E_g symmetry, which probes the *X* point of BZ we observe a feature of excitonic excitation at 16 meV. The extremely low width of 0.5 meV of the exciton feature in Al Flux-SmB₆ spectra suggests the extremely long life time of the level. The presence of Sm vacancies lead to a decrease of the exciton life time with eventual decay of the exciton through the electronic states present in the hybridization gap at of 1% of vacancies.

Our results suggest that an introduction of 1% of Sm vacancies while potentially changing Sm average valence has much larger effect on hybridization gap, preventing it from fully opening. The suppression of the hybridization gap by the presence of Sm vacancies can in turn suppress KTI state.

VI. ACKNOWLEDGEMENTS

We are grateful to C. Broholm, P. Nikolc, W. Fuhrman, J. Paglione, and N. P. Armitage for useful discussions. The work at IQM was supported by the U.S. Department of Energy, Office of Basic Energy Sciences, Division of Material Sciences and Engineering under Grant No. DE-FG02-08ER46544.

-
- [1] M. Dzero, K. Sun, V. Galitski, and P. Coleman, Phys. Rev. Lett. **104**, 106408 (2010).
 - [2] M. Dzero, K. Sun, P. Coleman, and V. Galitski, Phys. Rev. B **85**, 045130 (2012).
 - [3] V. Alexandrov, M. Dzero, and P. Coleman, Phys. Rev. Lett. **111**, 226403 (2013).
 - [4] S. Wolgast, i. m. c. b. u. i. e. i. f. Kurdak, K. Sun, J. W. Allen, D.-J. Kim, and Z. Fisk, Phys. Rev. B **88**, 180405 (2013).
 - [5] W. A. Phelan, S. M. Koohpayeh, P. Cottingham, J. W. Freeland, J. C. Leiner, C. L. Broholm, and T. M. McQueen, Phys. Rev. X **4**, 031012 (2014).
 - [6] P. Syers, D. Kim, M. S. Fuhrer, and J. Paglione, Phys. Rev. Lett. **114**, 096601 (2015).
 - [7] Z.-H. Zhu, A. Nicolaou, G. Levy, N. P. Butch, P. Syers, X. F. Wang, J. Paglione, G. A. Sawatzky, I. S. Elfimov, and A. Damascelli, Phys. Rev. Lett. **111**, 216402 (2013).
 - [8] J. Jiang, S. Li, T. Zhang, Z. Sun, F. Chen, Z. Ye, M. Xu, Q. Ge, S. Tan, X. Niu, M. Xia, B. Xie, Y. Li, X. Chen, H. Wen, and D. Feng, Nature Communications **4** (2013), 10.1038/ncomms4010.
 - [9] G. Travaglini and P. Wachter, Phys. Rev. B **29**, 893 (1984).
 - [10] H. Ohta, R. Tanaka, M. Motokawa, S. Kunii, and T. Kasuya, Journal of the Physical Society of Japan **60**, 1361 (1991).
 - [11] T. Nanba, H. Ohta, M. Motokawa, S. Kimura, S. Kunii, and T. Kasuya, Physica B: Condensed Matter **186188**,

- 440 (1993).
- [12] B. Gorshunov, N. Sluchanko, A. Volkov, M. Dressel, G. Knebel, A. Loidl, and S. Kunii, *Phys. Rev. B* **59**, 1808 (1999).
 - [13] K. Flachbart, K. Gloos, E. Konovalova, Y. Paderno, M. Reiffers, P. Samuely, and P. Švec, *Phys. Rev. B* **64**, 085104 (2001).
 - [14] I. Frankowski and P. Wachter, *Solid State Communications* **41**, 577 (1982).
 - [15] V. N. Antonov, B. N. Harmon, and A. N. Yaresko, *Phys. Rev. B* **66**, 165209 (2002).
 - [16] F. Lu, J. Zhao, H. Weng, Z. Fang, and X. Dai, *Phys. Rev. Lett.* **110**, 096401 (2013).
 - [17] W. T. Fuhrman, J. Leiner, P. Nikolić, G. E. Granroth, M. B. Stone, M. D. Lumsden, L. DeBeer-Schmitt, P. A. Alekseev, J.-M. Mignot, S. M. Koohpayeh, P. Cottingham, W. A. Phelan, L. Schoop, T. M. McQueen, and C. Broholm, *Phys. Rev. Lett.* **114**, 036401 (2015).
 - [18] W. A. Phelan, S. M. Koohpayeh, P. Cottingham, J. C. Leiner, M. D. Lumsden, X. P. Wang, C. Hoffmann, M. A. Siegler, and T. M. McQueen, Submitted to *Scientific Reviews*.
 - [19] M. Ezawa, Y. Tanaka, and N. Nagaosa, *Scientific reports* **3** (2013).
 - [20] T. P. Devereaux and R. Hackl, *Rev. Mod. Phys.* **79**, 175 (2007).
 - [21] E. Burstein, D. Mills, and R. Wallis, *Physical Review B* **4**, 2429 (1971).
 - [22] P. Nyhus, S. L. Cooper, Z. Fisk, and J. Sarrao, *Phys. Rev. B* **52**, R14308 (1995).
 - [23] P. Nyhus, S. L. Cooper, Z. Fisk, and J. Sarrao, *Phys. Rev. B* **55**, 12488 (1997).
 - [24] P. Alekseev, V. Lazukov, R. Osborn, B. Rainford, I. Sadikov, E. Konovalova, and Y. B. Paderno, *EPL (Europhysics Letters)* **23**, 347 (1993).
 - [25] W. T. Fuhrman and P. Nikolić, *Phys. Rev. B* **90**, 195144 (2014).
 - [26] M. Valentine and et al, Manuscript in preparation.
 - [27] T. Kasuya, K. Kojima, and M. Kasaya, in *Valence Instabilities and Related Narrow-Band Phenomena* (Springer, 1977) pp. 137–152.
 - [28] J. Freericks and T. Devereaux, *Physical Review B* **64**, 125110 (2001).
 - [29] I. Morke, V. Dvorak, and P. Wachter, *Solid State Communications* **40**, 331 (1981).
 - [30] P. Lemmens, A. Hoffmann, A. Mishchenko, M. Talantov, and G. Gntherodt, *Physica B: Condensed Matter* **206207**, 371 (1995).
 - [31] N. Ogita, S. Nagai, N. Okamoto, M. Udagawa, F. Iga, M. Sera, J. Akimitsu, and S. Kunii, *Phys. Rev. B* **68**, 224305 (2003).
 - [32] N. Ogita, S. Nagai, M. Udagawa, F. Iga, M. Sera, T. Oguchi, J. Akimitsu, and S. Kunii, *Physica B: Condensed Matter* **359361**, 941 (2005).
 - [33] R. Shuker and R. W. Gammon, *Phys. Rev. Lett.* **25**, 222 (1970).
 - [34] P. A. Alekseev, A. S. Ivanov, B. Dorner, H. Schober, K. A. Kikoin, A. S. Mishchenko, V. N. Lazukov, E. S. Konovalova, Y. B. Paderno, A. Y. Romyantsev, and I. P. Sadikov, *Europhysics Letters* **10**, 457 (1989).
 - [35] P. A. Alekseev *et al.*, *Physics-Uspekhi* **58** (2015).
 - [36] J. K. Freericks, T. P. Devereaux, M. Moraghebi, and S. L. Cooper, *Phys. Rev. Lett.* **94**, 216401 (2005).
 - [37] P. Thalmeier and P. Fulde, *Physical Review Letters* **49**, 1588 (1982).